Green-to-Red Photoconvertible Dronpa Mutant for Multimodal Super-resolution Fluorescence Microscopy

Benjamien Moeyaert,[†] Ngan Nguyen Bich,[†,⊥] Elke De Zitter,[†] Susana Rocha,[†] Koen Clays,[‡] Hideaki Mizuno,[§] Luc van Meervelt,[†] Johan Hofkens,[†] and Peter Dedecker*[,†]

[†]Department of Chemistry, KU Leuven, Celestijnenlaan 200F, bus 2404, 3001 Heverlee, Belgium, [‡]Department of Chemistry, KU Leuven, Celestijnenlaan 200D, bus 2425, 3001 Heverlee, Belgium, and [§]Department of Chemistry, KU Leuven, Celestijnenlaan 200G, bus 2403, 3001 Heverlee, Belgium [⊥]Present address: Chemistry Department, Hanoi National University of Education, 136-Xuan Thuy, Cau Giay, Hanoi, Vietnam.

ABSTRACT Advanced imaging techniques crucially depend on the labels used. In this work, we present the structure-guided design of a fluorescent protein that displays both reversibly photochromic and green-to-red photoconversion behavior. We first designed ffDronpa, a mutant of the photochromic fluorescent protein Dronpa that matures up to three times faster while retaining its interesting photochromic features. Using a combined evolutionary and structure-driven rational design strategy, we developed a green-to-red photoconvertible ffDronpa mutant, called pcDronpa, and explored different optimization strategies that resulted in its improved version, pcDronpa2. This fluorescent probe combines a high brightness with low photobleaching and photoblinking. We herein show that, despite its tetrameric nature, pcDronpa2 allows for multimodal subdiffraction imaging by sequentially imaging a given sample using both super-resolution fluctuation imaging and localization microscopy.

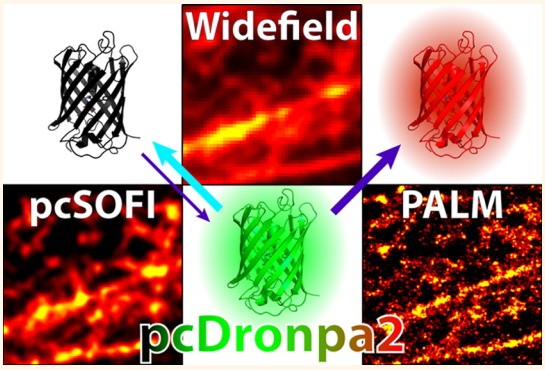

KEYWORDS: fluorescent proteins · Dronpa · protein engineering · crystal structure determination · super-resolution fluorescence microscopy · PALM · pcSOFI

Fluorescent proteins (FPs) and their applications in fluorescence microscopy have revolutionized cell biology.[1,2] The diversity of FPs has expanded dramatically with new labels that display dynamic fluorescence properties, such as photoactivation, photochromism, and photoconversion.[3,4] The great interest in these subclasses of FPs is mainly driven by the numerous applications in advanced fluorescence microscopy, including several approaches that allow fluorescence imaging beyond the diffraction limit.[5−7]

A broad range of super-resolution methodologies has been developed, based on the clever use of the fluorescence dynamics of "smart fluorophores", each providing different combinations of strengths and weaknesses.[8] This allows for a high degree of complementarity; for example, photoactivated localization microscopy (PALM)[9] offers a very high spatial resolution but poor temporal resolution and places high demands on the imaging quality, such as large photon doses with high signal-to-noise.[10,11] In contrast, photochromic stochastic fluctuation imaging (pcSOFI) offers a lower resolution improvement but better temporal resolution and is more tolerant of the imaging conditions (*i.e.*, high background, low signal, aberrations, *etc.*).[12,13]

Compared to traditional imaging, subdiffraction imaging contributes new layers of information, though it does so at the price of increased complexity, leading to new challenges in validation of the data. These challenges are apparent when considering the reliance on large data sets, extensive hands-off data processing, and/or strongly increased instrumental complexity. However, since different techniques will in general not be susceptible to the same artifacts, their combination can allow inconsistencies or artifacts to be revealed, or even addressed, with a much higher probability. The broader range of imaging conditions that is enabled by using multiple techniques

* Address correspondence to peter.dedecker@hotmail.com.

Received for review November 21, 2013 and accepted January 13, 2014.

Published online January 13, 2014
10.1021/nn4060144

can likewise contribute to experimental validation, by allowing more encompassing observations of the sample.

However, such complementary imaging is difficult, simply because different techniques place different demands on the fluorophore. For instance, localization microscopy achieves its highest spatial resolution with green-to-red photoconvertible fluorescent proteins due to the high photon dose from the red state, while pcSOFI uses labels that display reversible photochromism. The use of multiple fluorophores is not desirable, however, as introducing and validating even a single fluorophore in a biological system can require a large effort in terms of selection, generation, and validation, such as when creating transgenic organisms. As a result, the complementarity afforded by the different super-resolution imaging techniques remains constrained by the lack of labels with multimodal fluorescence properties, and comparatively little work has been performed on combining multiple photochemical behaviors into a single scaffold.

The history of directed evolution and semirational engineering of FPs is extensive. Reversibly photoswitchable FPs (RSFPs)[14−16] and several green-to-red photoconvertible FPs (PCFPs)[17−22] have been discovered, designed, and optimized, and recently, photoconvertible and biphotochromic FPs have been engineered.[23−25] Previously, we set the stage for the rational engineering of photoswitching behavior in photoconvertible FPs.[23] We now further expand this rational framework by semirationally introducing green-to-red photoconversion into a photochromic FP, by constructing a PCFP based on the well-known and extensively studied RSFP Dronpa.[26] Our results provide new insight into the process of photoconversion by linking structural data to spectroscopic and biochemical parameters. Moreover, the addition of this work to the already existing data on Dronpa and its mutants provides one of the most complete data sets for the study of structure and function of photoswitching and photoconversion. We also show that pcDronpa2 breaks new ground in super-resolution imaging by allowing independent and highly performing pcSOFI and PALM experiments on the same sample.

RESULTS AND DISCUSSION

ffDronpa. One of the major challenges in FP engineering is the difficulty to distinguish between mutations that represent evolutionary dead ends and mutants that contain the desired character but whose fluorescence needs to be rescued before this becomes apparent. We reasoned that this challenge could be alleviated by starting from a folding-optimized variant whose robustness allows observation of the fluorescence phenotype even in the presence of mutations that are detrimental to the folding process. These proteins, maturing faster and/or to a higher degree

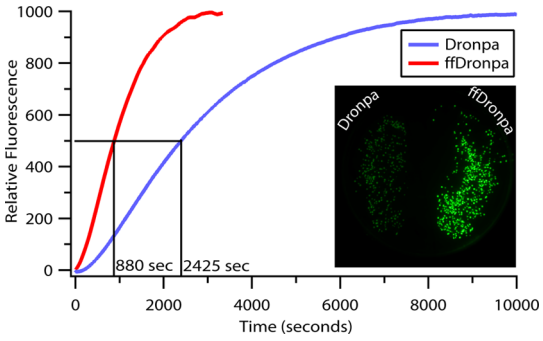

Figure 1. Maturation of Dronpa and ffDronpa. Time course of the relative fluorescence emission intensity of Dronpa and ffDronpa after *in vitro* translation recorded at 503 nm excitation and 517 nm emission. Inset: Fluorescence image of a bacterial culture plate expressing Dronpa (left) and ffDronpa (right) in *Escherichia coli* after 16 h of incubation at 37 °C.

of completeness, are known as "superfolder" FPs, and experimental strategies to generate these have been described previously.[27,28]

By observing the brightness of bacterial colonies expressing randomly mutated Dronpa genes, we identified Dronpa-V60A (Dronpa numbering used throughout the article; see Supporting Figure 1), a monomeric Dronpa mutant with increased in-colony brightness (Figure 1). *In vitro* maturation measurements showed that Dronpa-V60A forms almost three times faster than Dronpa, with a maturation half-time of less than 15 min (Figure 1). We thus called this mutant "fast-forming" or ffDronpa. Further characterization of the purified protein showed that Dronpa-V60A is spectroscopically identical to Dronpa, except for a slower photochromic response (Table 1). Given its improved properties, we expect that ffDronpa can be preferable to Dronpa in any labeling scheme involving moderately fast RSFPs.

pcDronpa. Although the mechanistic details of green−red photoconversion are still debated, the importance of the proton-binding and -donating capacities of the His62 imidazole group in PCFPs is well-recognized.[29−33] We thus introduced the His62 mutation in ffDronpa, resulting in a mutant protein that showed no detectable fluorescence. After a single round of random mutagenesis, we could identify a vaguely fluorescent colony (ffDronpa-C62H-N94S-N102I). A second round of random mutagenesis revealed a brightly fluorescent and effectively green-to-red photoconvertible mutant which we called pcDronpa (ffDronpa-C62H-N94S-N102I-E218G). Interestingly, of the six mutations that were introduced in the effort of creating monomeric Dronpa from its tetrameric ancestor 22G,[26] the residues at positions 102 and 218 are reversed in pcDronpa. Indeed, pcDronpa is a tetrameric protein, as supported by size-exclusion chromatography (Supporting Figure 2).

To probe the effect of the N94S mutation, we created pcDronpa-S94N and found it to be identical to pcDronpa. We also created ffDronpa-C62H-N94S, which was nonfluorescent and not distinguishable

TABLE 1. Photophysical Properties of All FPs Presented in This Work[a]

				pcDronpa		pcDronpa2		mEos3.2[37]		
	Dronpa[26]	22G[36]	ffDronpa	green	red	green	red	green	red	pcDronpa-A69T
λ_{ex} (nm)	503	507	503	505	569	504	569	507	572	494
λ_{em} (nm)	517	519	517	517	581	515	583	516	580	507
ε_1 (mM^{-1} cm^{-1})	[95]	[110]	105	115	75	100	105	[63.4]	[32.2]	34
ε_2 (mM^{-1} cm^{-1})	23	ND	22	19	NA	20	NA	ND	NA	22
QY_{fluo} (%)	76 [85]	[67]	75	85	68	83	68	76 [84]	65 [55]	82
brightness	72.2	73.7	78.8	97.8	51.0	83.0	71.4	[53]	[18]	27.9
pK_a	5.3	[4.7]	5.0	5.5	6.3	5.8	6.1	[5.4]	[5.8]	8.0
QY_{off} (10^{-6})	160	4.7	70	5.6	NA	13	NA	NA	NA	NA
QY_{on} (10^{-3})	165	ND	172	92	NA	97	NA	NA	NA	NA
switching contrast, cuvette (-fold)	38.4	2.36	25.2	3.67	NA	5.57	NA	NA	NA	NA
switching contrast, microscope (-fold)	24.4	12.4	15.0	13.9	NA	19.9	NA	NA	NA	NA
normalized photoconversion efficiency	NA	NA	NA	0.14	NA	2.56	NA	1	NA	NA

[a] Photophysical properties of Dronpa, 22G, ffDronpa, pcDronpa, pcDronpa2, and mEos3.2 in green and red form and pcDronpa-A69T. ε_1: extinction coefficient of the chromophore in its anionic state absorbing maximally around 500 nm for the green state and around 570 nm for the red state. ε_2: extinction coefficient of the chromophore in its neutral state absorbing maximally around 380 nm. Brightness = extinction coefficient × quantum yield. Switching contrast = $fluorescence_{on}/fluorescence_{off}$. Values between square brackets are taken from the literature cited in the first row. NA = not applicable. ND = not determined. The calculation and interpretation of the normalized photoconversion efficiency is described in the Methods section.

from ffDronpa-C62H. This leads us to conclude that the role of the N94S mutation is small, if any. We also evaluated the importance of the V60A folding mutation by constructing pcDronpa-A60V. This mutant matures markedly slower than pcDronpa and reaches full maturation only after several days of incubation at 4 °C, showing the usefulness of starting from a folding-enhanced template.

The green state of pcDronpa absorbs maximally at 505 nm, emits maximally at 517 nm (Figure 2a and Table 1), and has an excited state lifetime of 3.2 ns. Off- and on-switching can be achieved with 488 and 405 nm light, respectively (Figure 2b). While the off-switching quantum yield of pcDronpa is more than 25 times lower than Dronpa, the on-switching quantum yields are similar. The off-switching quantum yield, switching contrast (Table 1), and photofatigue (Supporting Figure 3) of pcDronpa are similar to 22G and likely a result of its tetrameric nature, as it has been shown that the A/C interface gains substantial structural disorder in the dark, nonfluorescent state, absent in tetramers.[34,35]

Irradiation of pcDronpa with high intensities of 405 nm light resulted in the formation of a red-emissive form. This red species absorbs maximally at 569 nm with emission peaking at 581 nm (Figure 2a and Table 1). The red state excited-state lifetime was measured to be 3.9 ns. SDS-PAGE revealed that photoconversion is accompanied by protein backbone cleavage, yielding fragments of about 11 and 18 kDa (Figure 2d), similar to what is found for other PCFPs.[38,39] Under the experimental conditions described in the Methods section, we could convert ~50% of the protein sample to the red state, at which point the rate of photodestruction of the red state due to the 405 nm light became dominant over the photoconversion (Supporting Figure 4). The graphs in Supporting Figure 4 are directly reminiscent of a two-step first-order consecutive mechanism (A → B → C) in which A is the green state, B the red state, and C the bleached red state, with fixed rate constants for both transitions. Although the green state shows clear photoswitching, we could not detect reversible photoswitching of the red form after irradiation with 561 nm light (up to 0.5 W/cm^2 in cuvette and 0.8 kW/cm^2 on the microscope).

Structure of pcDronpa. We determined the pcDronpa crystal structure in the fluorescent green-on, nonfluorescent green-off, and red state (PDB ID: 4HQ8, 4HQ9, and 4HQC). The structures were determined to a resolution of 1.95, 2.07, and 2.05 Å, respectively (Supporting Table 1). The overall structure and quaternary organization of pcDronpa is similar to Dronpa,[15] 22G,[40] DsRed,[41] and other FPs. An extension of the C-terminal tail forms dimers *via* an arm-in-arm configuration[42] (Figure 3a): a clasp region that interacts centrosymmetrically with the neighboring protomer chain. This configuration requires the torsional freedom that is contributed by the glycine residue at position 218. Moreover, a negatively charged moiety at this specific position might be affected by electrostatic repulsion by Glu140 and Asp192. In the tetrameric arrangement of the Dronpa monomers in the crystal structure (PDB 2Z6Z), one can see that Glu218 is facing outward, which is thought to prevent the arm-in-arm configuration observed in 22G and pcDronpa. The A/C interface is further stabilized by hydrophilic interactions, while the A/B interface is formed by a hydrophobic pocket containing the Ile102 we introduced (Supporting Figure 5). The crystal structure thus provides a complete explanation of how N102I and E218G lead to a tetrameric organization.

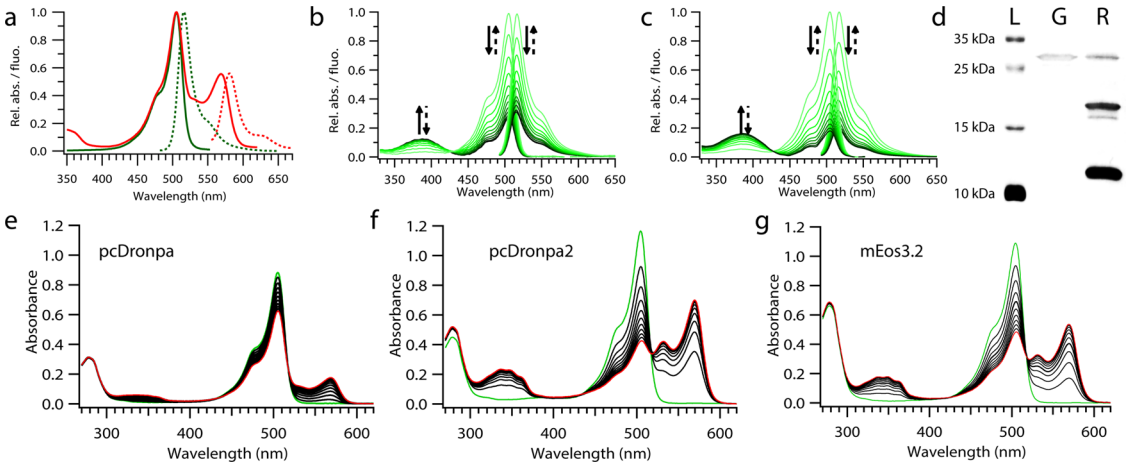

Figure 2. Spectroscopic and SDS-PAGE analysis of the photoswitching and photoconversion of pcDronpa(2). (a) Steady-state excitation ($\lambda_{det,G}$ = 555 nm, $\lambda_{det,R}$ = 625 nm; solid line) and emission ($\lambda_{ex,G}$ = 480 nm, $\lambda_{ex,R}$ = 550 nm; dotted line) of pcDronpa in the green and partially photoconverted red state. The green state excitation spectrum was scaled to unity at 505 nm, and emission was scaled to match the excitation maximum of the respective state. (b,c) Absorption and emission spectra (λ_{ex} = 488 nm) taken during the photoswitching (full arrows) of (b) pcDronpa and (c) pcDronpa2 from the green-on state (green line) to the green-off state (black line). In the reverse process (dotted arrows, spectra not shown), the spectra recover to the initial state. (d) SDS-PAGE of pcDronpa2 in both the green and red state. (e−g) Absorption spectra taken during photoconversion of (e) pcDronpa, (f) pcDronpa2, and (g) mEos3.2 from the green-emissive (green line) to the red-emissive (red line) state.

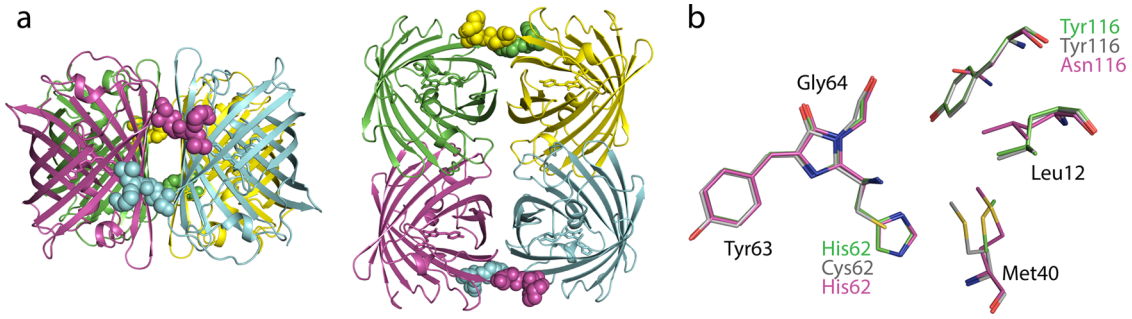

Figure 3. Quaternary structure and chromophore environment of pcDronpa. (a) Cartoon representation of a tetramer of pcDronpa (side and top view) showing the arm-in-arm configuration of the C-terminal tails (filled spheres). Each monomer is represented by a different color. (b) Comparison of the chromophores and conformations of residues Met40, Leu12, and Tyr/Asn166 in Dronpa (gray, PDB ID: 2Z1O), pcDronpa (green, PDB ID: 4HQ8), and EosFP (magenta, PDB ID: 1ZUX). Color code: oxygen in red; nitrogen in blue; carbon in green, gray, and magenta in pcDronpa, Dronpa, and EosFP, respectively.

The chromophores of Dronpa and the green state of pcDronpa in their fluorescent form have similar conformations, with the *p*-hydroxyphenyl ring in a *cis* configuration and coplanar with the imidazolinone ring (Figure 3b, Figure 4a, and Supporting Figure 6a, tilt and twist angles[43] of 11.9 and −17.1°, respectively). The only appreciable conformational difference in the chromophore environment of pcDronpa compared to Dronpa is Met40, whose sulfur atom is displaced by 0.94 Å (Figure 3b), allowing the imidazole moiety of His62 to fit.

The pcDronpa green-off state, which was obtained by switching off the fluorescence *in crystallo* through irradiation at 491 nm, shows the chromophore in a *trans* configuration (Figure 4a and Supporting Figure 6b, tilt and twist angles of 153.7 and 53.7°, respectively). Also evident from the crystal structure are rearrangements in the His193 and Arg66 residues, which support and provide space for the isomerized chromophore. The Cα atoms of Val157, Asn158, and Met159, part of the β-8 strand, are displaced by 0.6, 0.8, and 0.3 Å, respectively. These differences between the bright and dark state structures of pcDronpa match earlier observations on Dronpa.[44]

The structure of pcDronpa in the red-on state was determined by crystallizing a photoconverted protein sample. In order to avoid the inclusion of photobleached molecules, the concentrated protein sample was converted only to 40−50% completeness as determined by absorption measurements. The backbone cleavage between the Cα and the Nα of His62, typical for a PCFP red state chromophore[29−31] (Figure 4b), is clearly visible (Supporting Figure 6c,d). The occupancy factor of 0.39 (averaged from 6 monomers in an asymmetric unit) for this red form obtained from the refinement corroborates the estimated conversion completeness of the initial protein sample.

The red state chromophore of pcDronpa is less planar (tilt and twist angles of 14.5 and −28.6°,

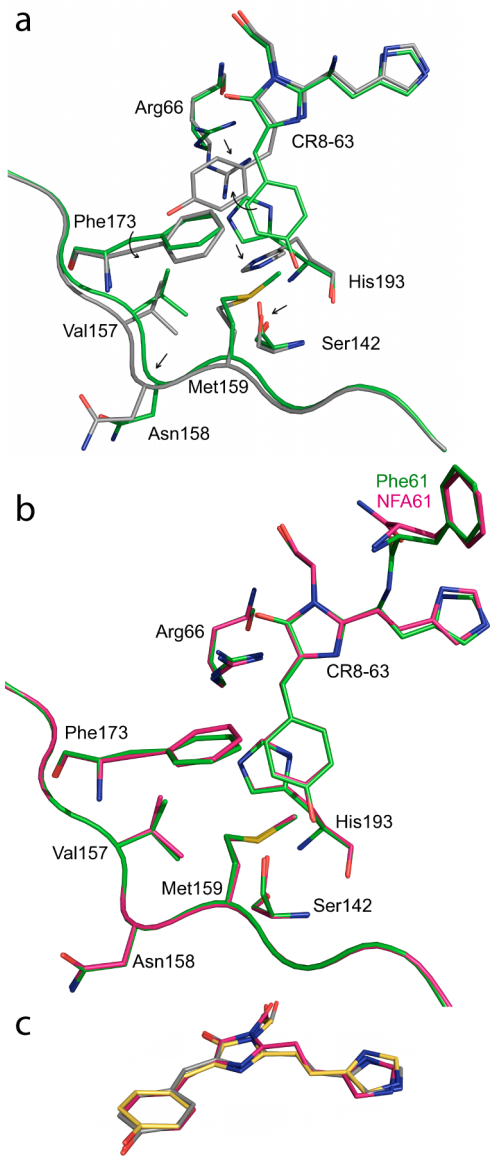

Figure 4. Structural effects of photoswitching and photoconversion in pcDronpa. (a) Comparison of the chromophore and its environment in the green-on (green) and green-off (gray) states of pcDronpa. The arrows show the rearrangement of the corresponding residues. (b) Superposition of the chromophores of the green-on (green) and red-on (red) states of pcDronpa, clearly showing the cleavage backbone. Residues are shown in stick format, β-strand 8 is shown in tube representation, and residues on β-strand 8 are represented by their side chains only. (c) Superposition of the red-on chromophores of pcDronpa (red), Kaede (gray), and IrisFP (yellow). Color code: oxygen in red; nitrogen in blue; carbon in the color corresponding with the color of the respective protein.

respectively) compared to its green-on state and the red state of other PCFPs, as illustrated for Kaede and IrisFP in Figure 4c. This nonplanarity is likely due to a hydrophobic interaction of the imidazole group of the red state chromophore with the Met40 moiety, which has a markedly different conformation in pcDronpa compared to Dronpa. Saturation mutagenesis of Met40 did not result in mutants with improved photoconversion properties.

We further investigated the origins of the absence of photoswitching in the red state. As can be seen from Figure 4b, the residues surrounding the chromophore of pcDronpa do not show pronounced conformational differences between the green and red state. The only immediately apparent conformational difference can be found in the nonplanarity of the double bond at the histidine end of the chromophore in the red state.

For IrisFP, which does photoswitch in the red state, we measured an excited-state lifetime of 3.5 ns for the red state, and a fluorescence quantum yield of 0.47 was previously reported.[25] This is significantly lower than the excited-state lifetime of 3.9 ns and fluorescence quantum yield of 0.68 for the red form of pcDronpa. This corresponds to a decrease of the rate constant for nonradiative decay from 1.5×10^8 to 8.3×10^7 s^{-1} from IrisFP to pcDronpa in the red state. Together with the observed nonplanarity and the more narrow absorption and emission bands observed for pcDronpa (Figure 2f) in comparison to IrisFP,[25] this lower value suggests a smaller conformational mobility (or amplitude of low frequency vibrations like, *e.g.*, internal rotations) for pcDronpa possibly due to a tighter packing. This suggests that it is not the static nature of the structure that impedes the photoswitching, but rather the reduced rotational freedom of the chromophore.[45]

pK_a Engineering. It is generally accepted that the green-to-red photoconversion process occurs from a protonated state of the chromophore. We sought to improve the photoconversion efficiency of pcDronpa by increasing the pK_a of the chromophore using rational design, as has been suggested previously.[46] We made pcDronpa-A69T and confirmed a pK_a of 8.0 compared to 5.5 in pcDronpa. The origins of this shift were elucidated by obtaining a crystal structure of pcDronpa-A69T at 2.15 Å resolution (Supporting Table 1, PDB ID: 4IZN). From this structure, we see that in pcDronpa-A69T the interaction of Arg66 with the keto group of the chromophore's imidazolinone moiety is no longer present. As such, negative charges on the chromophore are less stabilized and the pK_a is higher. This situation is similar to that observed in Dendra2 (Supporting Figure 7), which has a pK_a of 7.1[46] compared to 6.1 in Dendra2-T69A. The A69T mutation markedly lowered pcDronpa's brightness, largely due to a lower extinction coefficient, and resulted in a hypsochromic shift of the absorption and emission wavelengths of about 10 nm (Table 1). This shift can be explained by the absence of the guanidinium group of Arg66, which otherwise stabilizes the chromophore's imidazolinone group. While at pH 7.4 the extinction coefficient of pcDronpa-A69T in the protonated state is relatively high, we could not detect any photoconversion to a red state. We thus conclude that there is no simple one-to-one correlation between the pK_a of the chromophore's hydroxyphenyl group and the photoconversion efficiency. This is in accordance with recent studies

pointing out that the charge states of the amino acids surrounding the chromophore rather than the chromophore's pK_a are determining the photoconversion rate.[47]

pcDronpa2. In a different approach to improve the photoconversion efficiency, we aligned the crystal structures of pcDronpa and several PCFPs and found that the most particular discrepancy in the chromophore environment was situated at position 116. This position is occupied by Tyr in pcDronpa, but by Asn in Kaede, EosFP, KikGR, and mMaple and by Gln in Dendra2. Among the non-photoconvertible FPs, this position is not well-conserved. The region occupied by the hydroxyl group of Tyr116 in pcDronpa contains a water molecule in the other PCFPs, except for Dendra2, where this region is occupied with the O_ε of Gln116 (Supporting Figure 8). This water molecule, amide oxygen (in case of Dendra2), or hydroxyl group (in case of pcDronpa) is in direct contact with another water molecule (W412 in pcDronpa) that is within hydrogen bonding distance of the N_δ of the chromophore His62. This hydrogen bonding network has been suggested to be crucially important for photoconversion.[29−31,47] Moreover, the water molecule that is present in the green, but not the red form in EosFP (W1171), IrisFP (W2077), and Kaede (W459), commonly referred to as W1, is absent in all pcDronpa crystal structures. It was suggested that this water molecule is actively participating in the photoconversion,[31] which could be at the basis of pcDronpa's low photoconversion efficiency, although others have suggested that this W1 is not crucial for the photoconversion.[30]

We performed saturation mutagenesis on position 116 and identified a mutant with markedly enhanced photoconversion efficiency. This mutant, which we called pcDronpa2, contains Asn at position 116, is switchable in the green form (Figure 2c), and has a considerably increased photoconversion rate compared to pcDronpa (Figure 2f). While it was, due to the low absorption at 405 nm, impossible to determine the quantum yield of green-to-red photoconversion of pcDronpa2 with satisfactory accuracy, we calculated a normalized photoconversion efficiency that can be used to compare the ease of photoconversion across different proteins (Figure 2g and Table 1). For both pcDronpa2 and mEos3.2, we could achieve a photoconversion completeness of ~60%, after which the rate of photodestruction of the red state became dominant over the photoconversion (Supporting Figure 4). The increased green-to-red photoconversion efficiency is most likely explained by a rearrangement of the hydrogen bonding network surrounding the histidine moiety of the chromophore. We also introduced a Gln residue at position 116 of pcDronpa, as is the case in Dendra2. While pcDronpa-Y116Q had a pK_a of 6.8, the photoconversion efficiency was similar to pcDronpa-Y116N (pcDronpa2). Yet again, pK_a does not seem to be a good indicator of green-to-red photoconversion efficiency.

The red form of pcDronpa2 has the highest extinction coefficient of all PCFP red forms known to date (105 000 M^{-1} cm^{-1}) and is, just like its ancestor pcDronpa, not photoswitchable in the red form. Rational mutagenesis based on literature examples (S142A, V157I/G/S, M159A/T, F173S/L)[15,23,45,48] did not generate a four-way highlighter pcDronpa2 mutant (data not shown).

We measured the quantum yield of (irreversible) photobleaching (experimental conditions described in the Methods section) of the red form of pcDronpa2 (1.66×10^{-6}) and mEos3.2 (1.93×10^{-5}) in a cuvette. Under these conditions, the red form of pcDronpa2 appeared to be more than 10 times more photostable than mEos3.2. However, these measurements are performed at relatively low illumination power (0.5 W/cm^2) and in buffer, which means that they cannot be directly translated to the performance in a microscopic setting. We therefore recorded and analyzed wide-field data on the photostability and photoblinking of pcDronpa2 and mEos3.2 (see Methods section for experimental details) and found that, under these conditions, the red-emissive state of pcDronpa2 is as photostable as mEos3.2 in the red state while being slightly less prone to photoblinking (Supporting Figure 9). We believe that the discrepancy between the data recorded in cuvette and on the microscope is due to a nonlinear dependency of photobleaching on the illumination power.[49]

Monomerization of pcDronpa2. We found that reverting the N102I and E218G mutations is not a viable strategy to obtain a monomeric pcDronpa2 variant. ffDronpa-C62H-N94S turned out to be nonfluorescent, and ffDronpa-C62H-N94S-N102I is only very dimly fluorescent. As an alternative approach, we used our crystallographic data to rationally break the tetramer interfaces in a different way (see Supporting Figure 5). Mutations N158E and Y188A disrupted the A/C interface, while V123T additionally broke the A/B interface (see Supporting Figure 2). Although we could thus successfully make a monomeric version of pcDronpa2 (pcDronpa2-V123T-N158E-Y188A), this mutant displayed no photoconversion. While a range of monomeric PCFPs is available and actively used,[18−20,37,50] our data and literature examples alike[21,39] demonstrate that PCFPs are often found in a tetrameric organization and tend to resist monomerization. Clearly, this oligomeric nature influences green-to-red photoconversion rather strongly, though the structural origins responsible for this effect are unclear.

Microscopy. We sought to evaluate the use of pcDronpa2 for multimodal diffraction-unlimited fluorescence microscopy. Upon transfection with a plasmid encoding pcDronpa2 fused to human β-actin, fixed HeLa cells displayed a bright fluorescence distribution characteristic of the actin cytoskeleton. Upon irradiation with 488 nm light, we observed a rapid decrease in green fluorescence intensity, consistent with the photochromic nature of pcDronpa2, quickly reaching a plateau characterized by rapid and

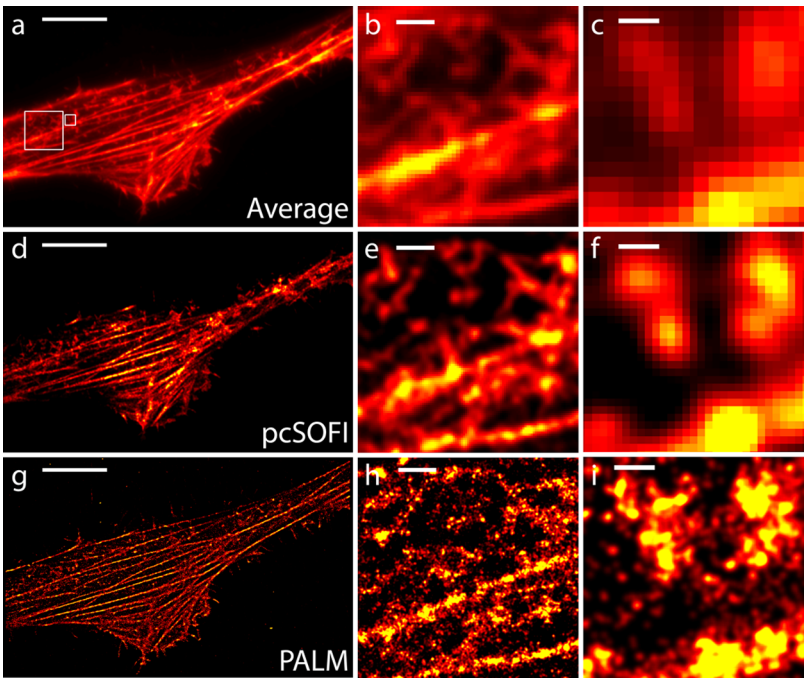

Figure 5. Microscopic imaging of pcDronpa2-tagged human β-actin. (a−c) Wide-field image of pcDronpa2-labeled β-actin in HeLa cells made by averaging the 700 frames used in pcSOFI. (d−f) pcSOFI image of the same cell. (g−i) PALM image of the same cell. The scale bar in frames a, d, and g is 10 μm. Frames b, e, and h show a detail of the β-actin structure (scale bar = 1 μm). Frames c, f, and i are further zoomed in (scale bar = 0.3 μm). The absence of some actin fibers at the outer edges of the cell in the pcSOFI image is due to the increased *z*-sectioning in pcSOFI combined with imperfections of the 488 nm illumination and these structures being slightly out of focus.

stochastic intensity fluctuations, similar to the blinking behavior previously reported on Dronpa and rsTagRFP.[12,51] We acquired 700 images over approximately 35 s and subjected these to a second-order cross-cumulant pcSOFI analysis (Figure 5d). The resulting images displayed a 2-fold increase in spatial resolution and marked increase in detail (Figure 5e,f).

Next, we switched to PALM imaging of the very same cell, by reconfiguring the instrument for the detection of red fluorescence and converting the green state proteins to the red state using 405 nm light during the acquisition. Individual pcDronpa2 molecules could be clearly observed over more than 25 000 acquired images and were recorded and analyzed to an estimated precision of 22 nm (2.6×10^6 total localizations, 6.4×10^5 consolidated localizations). The high-resolution reconstructed images (Figure 5g−i) show a very high increase in detail that is consistent with the pcSOFI images. Importantly, this consistency allows us to additionally validate the results obtained by both techniques, adding further confidence to the recorded images.

CONCLUSIONS

In this work, we have developed a novel fluorescent highlighter probe based on the photochromic fluorescent protein Dronpa and demonstrated its usefulness in multimodal super-resolution fluorescence microscopy, combining pcSOFI with PALM. We first identified ffDronpa, a Dronpa variant that forms up to three times as fast as Dronpa, while retaining its interesting photochromic properties. In our hands, ffDronpa is the label of choice for experiments involving moderately fast reversibly photoswitchable fluorescent proteins.

After rationally introducing His62 in ffDronpa and two rounds of random mutagenesis, we identified the effectively green-to-red photoconvertible pcDronpa. It is the first three-way optical highlighter that combines reversible photochromism in the green state with photoconversion to a non-photochromic red state. We obtained crystal structures of the green-on, green-off, and red state.

Using this structural data, we sought to improve pcDronpa's photoconversion efficiency. In a first attempt, we rationally increased the pK_a of the chromophore but found that this is not a viable strategy for improving the photoconversion efficiency. A second strategy involved mutating residue 116 to Asn. This resulted in pcDronpa2, a mutant that is very efficiently photoconvertible, comparable to mEos3.2 and has the brightest red state of all known green-to-red PCFPs. Together with the absence of switching in the red state, this makes pcDronpa2 a very interesting probe for PALM imaging. By rationally breaking the A/B and A/C interface, we turned pcDronpa into a monomeric, albeit non-photoconvertible fluorescent probe. Thus far, we have not be able to obtain a monomeric and photoconvertible pcDronpa variant.

We herein show that pcDronpa2 opens doors for multimodal super-resolution imaging of biological

samples, due to its tailored "smart" properties. At the cost of having to use a tetrameric label, we have shown that pcDronpa2 allows one to combine pcSOFI and PALM super-resolution imaging, leading to a more flexible, streamlined, and verifiable approach toward fluorescence imaging beyond the diffraction limit.

METHODS

Cloning, Library Construction, and Screening. Rational mutagenesis was performed as previously described.[52] A list of primers is available as Supporting Information (Supporting Table 2). For random mutagenesis, a similar megaprimer-based protocol was used.[53] All cloning and protein expression was done using the pRSet-B vector (Invitrogen) with the insert cloned between the *Bam*HI and *Eco*RI sites in *E. coli* JM109(DE3) cells (Promega). To screen for photoconversion, bacterial plates were incubated at 4 °C on a home-built 405 nm LED source and illuminated overnight. Red fluorescent colonies were readily visible under 488 nm light illumination, picked, grown, miniprepped, and sequenced (LGC Genomics).

For the visualization of human β-actin, the KikGR gene was replaced by the gene coding for pcDronpa in the phKikGR-I-MCI vector (Amalgaam) using primers Dronpa_NheI_actin_FWD and Dronpa_AgeI_actin_REV and standard cloning between the NheI and the AgeI site.

Protein Purification and Characterization. Proteins were purified as described in Supporting Method 1. Extinction coefficients were measured by Ward's method[54] using the literature value of Dronpa (95 mM^{-1} cm^{-1}) as a reference. The quantum yields of fluorescence were determined relative to fluorescein in 0.1 M NaOH (QY = 0.925) for the green form and relative to rhodamine6G in TN buffer (QY = 0.92) for the red form. Both absorption and emission were measured with the setup used for photoactivation analysis described below, equipped with an extra 473 nm (50 mW, Spectra Physics) or 532 nm (200 mW, Spectra Physics) laser for excitation. The pK_a values were measured by calculating the inflection point of the sigmoids that were fitted (Igor Pro, Wavemetrics) to the absorption maxima of the neutral and anionic species at pH values ranging from 3 to 13.

The protocol for measuring the maturation speed was largely based on a previously described method.[55] Plasmid DNA was mixed with all necessary components for *in vitro* translation (PURExpress *in vitro* protein synthesis kit, NEB) in a volume of 25 μL and incubated at 37 °C for 15 min and afterward immediately frozen and stored at −80 °C. The sample was taken out of the freezer, and immediately, 150 μL of air-saturated maturation buffer consisting of 50 mM Tris-HCl, 2 mM $MgCl_2$, 35 mM KCl, 5 mM β-mercaptoethanol, and 0.3 mg/mL chloramphenicol at pH 7.5 and 37 °C was added to the sample. The solution was immediately transferred to a PTI QuantaMaster fluorimeter which was set at 503 nm excitation and kept at 37 °C. Emission at 518 nm was measured every second until a plateau value was reached.

The setup that was used for determining the photoactivation behavior of the fluorescent proteins is schematically represented and discussed in Supporting Figure 10. For photoswitching experiments, the protein samples were diluted in 1 mL of TN buffer to an optical density of below 0.2 at the absorption maximum. The cuvette (Hellma) was kept at 10 °C and continuously stirred. For off- and on-switching, a 488 nm Ar-ion gas laser (Spectra Physics) operating at 0.5 W/cm^2 and a 405 nm diode laser (Coherent CUBE) operating at 0.047 W/cm^2 were directed into the cuvette from above. For photoconversion, the protein sample was diluted to an optical density of between 1.0 and 1.5 at the absorption maximum and subsequently irradiated with the 405 nm diode laser at higher laser power (1 W/cm^2). The normalized photoconversion efficiency was calculated as the initial slope of the reduction in green state absorbance divided by the initial concentration of the green state, after which all values were normalized to the value obtained for mEos3.2. The normalized photoconversion efficiency is a measure for the ease of photoconversion that contains both the green state absorption at 405 nm and the quantum yield of photoconversion and is independent of the intensity of 405 nm irradiation. Using a 561 nm DPSS laser (Cobolt Jive) operating at 0.5 W/cm^2, we irradiated the photoconverted protein samples to check for photoswitching in the red form. For photobleaching of the red state, the photoconverted sample was diluted to an OD of 0.2−0.4 at the maximum absorption wavelength and irradiated with 561 nm light (0.5 W/cm^2) while absorption spectra were recorded every minute.

The data were fitted to the model derived and described in detail in Supporting Method 2, from which the quantum yields of off-switching, on-switching, and photobleaching could be calculated. Excited-state lifetime data were measured and analyzed as described elsewhere.[23] The excitation wavelength was 488 and 560 nm for the green and red state, respectively. Emission wavelengths varied between 505 and 580 nm and 575 and 650 nm for the green and red state, respectively.

For the analysis of photoswitching fatigue and photoswitching contrast under high illumination powers, we used a setup that consisted of a Sola Light Engine (Lumencor) coupled into an inverted microscope (Olympus IX71) equipped with a zt488rdc dichroic mirror (Chroma) and a 10× objective (UplanSApo, Olympus). Fluorescence images were recorded using an EMCCD camera (iXon, Andor). For the photofatigue measurements, a suspension of NiNTA beads (Qiagen) covered in His6-tagged FPs was sandwiched between two coverslips. The proteins were switched off to 5% of their initial emission with cyan light and back to the on-state with violet light. This cycle was repeated 100 times. For photoswitching contrast on the microscope, samples were prepared in a thin film of polyacrylamide as described before.[16] Proteins were switched off with cyan light until a plateau value was reached; the camera background was subtracted, and the ratio between the average initial and final pixel value was calculated.

The oligomerization state of the proteins was analyzed by size-exclusion chromatography (SEC) at a concentration of 0.1 mM in TN buffer. We used a HiLoad Superdex 200 pg 16/600 column coupled to an Akta Purifier 10 system (both GE Healthcare) that was calibrated with a gel filtration molecular weight marker kit (MWGF200, Sigma Aldrich).

Crystallography. Crystallization conditions of pcDronpa and pcDronpa-A69T were screened for using the 96-matrix Index screen (Hampton Research) by the sitting-drop vapor-diffusion method. Promising conditions were consequently prepared manually in sitting drops consisting of 1.5 μL of pcDronpa (7 mg/mL) or pcDronpa-A69T (5 mg/mL) protein solution in 0.1× TN buffer and 1.5 μL of the well solution and were placed against 100 μL of the screening solution at 16 °C. Yellow-greenish pcDronpa crystals were obtained after approximately a week in a condition of 25% (w/v) PEG 3350, 0.1 M HEPES pH 7.5. The green-off crystals were obtained by irradiating the yellow-greenish crystals with a 488 nm laser for 5−10 min in a dark room. The crystals were clearly dimmer (essentially colorless) compared to the nonilluminated ones. To obtain the red-on crystals, we irradiated the pcDronpa solution in optimal conditions for photoconversion, in which the maximal effectiveness for the photoconversion of pcDronpa was about 40−60%. We used this red solution for crystallization. Red crystals appeared in the same condition and after the same period as the yellow-greenish ones. Plate-like crystals of pcDronpa-A69T were grown in a condition of 32% (v/v) PEP 426, 0.05 M HEPES pH 8.0, and 0.2 M KCl. Prior to X-ray data collection, the crystals were flash-frozen in liquid nitrogen without using cryoprotectants. Details about the X-ray diffraction data acquisition, structure determination, and refinement can be found in Supporting Method 3.

Microscopy. For both the human β-actin- and the membrane-targeted constructs, the plasmid DNA was transfected into

cultured HeLa cells using the calcium phosphate method (Molecular Cloning), grown in DMEM medium supplemented with 10% FBS, glutamax, and gentamicin (all Gibco) on glass-bottom dishes (MatTek). Green fluorescence was clearly visible 24−72 h after transfection. Cells were washed three times with HBSS medium (GIBCO) that was preheated to 37 °C, fixed with freshly prepared and preheated 4% formaldehyde in PBS for 30 min at 37 °C, washed three times with PBS, and then stored at 4 °C for no longer than 2 weeks until the samples were imaged.

We used an Olympus IX83 inverted microscope equipped with a cell^tirf module, a 100 mW 405 nm, a 150 mW 488 nm, and a 150 mW 651 nm cell* laser, a UAPON 150XOTIRF objective, manufacturer-installed filters (all Olympus), and an EMCCD camera (Hamamatsu ImagEM). In the cell^tirf module, ND2 and ND1 filters (Thorlabs) were inserted in the 405 and 488 nm lines, respectively. The exposure time of the camera was set at 50 ms with an EM gain of 500. After acquiring 1000 frames of green fluorescence for pcSOFI analysis, 25 000 frames of PALM data were acquired. Data analysis was done with the Localizer package[56] with empirically optimized settings. The estimated localization precision was determined by consolidating the identical emitters and multiplying the pixel size with the computationally estimated localization error.

For the analysis of photostability of the red form of pcDronpa2 and mEos3.2, samples of HeLa cells expressing FP-labeled human β-actin were imaged like for PALM imaging. The total integrated intensity of the fitted positions of the red state emitters was calculated using the "Consolidate identical emitters" function of Localizer. Molecules that were emitting for more than 5 frames were discarded, as they can be considered fluorescent impurities of the sample. The intensity histograms of eight data sets were evaluated, and it was seen that discarding localizations that were emitting more than 5 frames reduced the weight of the tail of the distribution without altering the distribution maximum. This shows that the tail intensities are mostly independent from the fluorescent proteins. For each FP label, eight independent data sets of 7500 frames each were analyzed and summed.

Photoblinking was quantified using similar samples as for the photostability analysis, but during acquisition, the intensity of the 405 nm laser was reduced more than 100-fold such that only 10−20 molecules were on in any given frame. Molecules that were on for more than 5 consecutive frames were again discarded. For every molecule, we calculated the number of times it blinked, that is, went to a dark state and subsequently recovered to a bright state. These data were plotted in a normalized histogram.

Conflict of Interest: The authors declare no competing financial interest.

Acknowledgment. The research leading to these results has received funding from the European Research Council under the European Union's Seventh Framework Programme (FP7/2007-2013 ERC Grant Agreement No. 291593 FLUOROCODE), from the Flemish government in the form of long-term structural funding (Methusalem Grant METH/08/04 CASAS), from the Research Foundation−Flanders (FWO) (Grants G.0197.11 and G0484.12) and from the Hercules Foundation (HER/08/021). The authors thank M. Van der Auweraer for fruitful discussions, E. Fron for help with the lifetime measurements, the staff of the Swiss Light Source in Villigen (beamline PXIII) for help with the synchrotron experiments, and S. Strelkov and S. Beelen for the technical assistance. B.M. is funded by a Ph.D. grant from the Agency for Innovation by Science and Technology (IWT) Flanders. N.N.B. was funded by a Ph.D. grant from the Vietnamese Government (project 322). P.D. is a postdoctoral fellow of the Research Foundation−Flanders (FWO).

Supporting Information Available: Details about the protein purification, calculation of the photoswitching and photobleaching quantum yield and crystallographic details. Crystallographic data collection and refinement parameters, list of primers, alignment and numbering of proteins, size-exclusion chromatography results, photofatigue, absorption during photoconversion, photostability, and blinking data. Details about the crystal structures. This material is available free of charge *via* the Internet at http://pubs.acs.org.

REFERENCES AND NOTES

1. Miyawaki, A. Proteins on the Move: Insights Gained from Fluorescent Protein Technologies. *Nat. Rev. Mol. Cell Biol.* **2011**, *12*, 656–668.
2. Chudakov, D. M.; Matz, M. V.; Lukyanov, S.; Lukyanov, K. A. Fluorescent Proteins and Their Applications in Imaging Living Cells and Tissues. *Physiol. Rev.* **2010**, *90*, 1103–1163.
3. Shaner, N. C.; Patterson, G. H.; Davidson, M. W. Advances in Fluorescent Protein Technology. *J. Cell Sci.* **2007**, *120*, 4247–4260.
4. Lukyanov, K. A.; Chudakov, D. M.; Lukyanov, S.; Verkhusha, V. V. Photoactivatable Fluorescent Proteins. *Nat. Rev. Mol. Cell Biol.* **2005**, *6*, 885–891.
5. Dedecker, P.; Hofkens, J.; Hotta, J. Diffraction-Unlimited Optical Microscopy. *Mater. Today* **2008**, *11*, 12–21.
6. Hell, S. W. Far-Field Optical Nanoscopy. *Science* **2007**, *316*, 1153–1158.
7. Zhou, X. X.; Lin, M. Z. Photoswitchable Fluorescent Proteins: Ten Years of Colorful Chemistry and Exciting Applications. *Curr. Opin. Chem. Biol.* **2013**, *17*, 682–690.
8. Dedecker, P.; Schryver, F. C.; De Hofkens, J. Fluorescent Proteins: Shine on, You Crazy Diamond. *J. Am. Chem. Soc.* **2013**, *135*, 2387–2402.
9. Betzig, E.; Patterson, G. H.; Sougrat, R.; Lindwasser, O. W.; Olenych, S.; Bonifacino, J. S.; Davidson, M. W.; Lippincott-Schwartz, J.; Hess, H. F. Imaging Intracellular Fluorescent Proteins at Nanometer Resolution. *Science* **2006**, *313*, 1642–1645.
10. Patterson, G.; Davidson, M.; Manley, S.; Lippincott-Schwartz, J. Superresolution Imaging Using Single-Molecule Localization. *Annu. Rev. Phys. Chem.* **2010**, *61*, 345–367.
11. Bates, M.; Huang, B.; Zhuang, X. Super-resolution Microscopy by Nanoscale Localization of Photo-switchable Fluorescent Probes. *Curr. Opin. Chem. Biol.* **2008**, *12*, 505–514.
12. Dedecker, P.; Mo, G. C. H.; Dertinger, T.; Zhang, J. Widely Accessible Method for Superresolution Fluorescence Imaging of Living Systems. *Proc. Natl. Acad. Sci. U.S.A.* **2012**, *109*, 10909–10914.
13. Dertinger, T.; Colyer, R.; Iyer, G.; Weiss, S.; Enderlein, J. Fast, Background-Free, 3D Super-resolution Optical Fluctuation Imaging (SOFI). *Proc. Natl. Acad. Sci. U.S.A.* **2009**, *106*, 22287–22292.
14. Bizzarri, R.; Serresi, M.; Cardarelli, F.; Abbruzzetti, S.; Campanini, B.; Viappiani, C.; Beltram, F. Single Amino Acid Replacement Makes *Aequorea victoria* Fluorescent Proteins Reversibly Photoswitchable. *J. Am. Chem. Soc.* **2010**, *132*, 85–95.
15. Stiel, A. C.; Trowitzsch, S.; Weber, G.; Andresen, M.; Eggeling, C.; Hell, S. W.; Jakobs, S.; Wahl, M. C. 1.8 A Bright-State Structure of the Reversibly Switchable Fluorescent Protein Dronpa Guides the Generation of Fast Switching Variants. *Biochem. J.* **2007**, *402*, 35–42.
16. Grotjohann, T.; Testa, I.; Leutenegger, M.; Bock, H.; Urban, N. T.; Lavoie-Cardinal, F.; Willig, K. I.; Eggeling, C.; Jakobs, S.; Hell, S. W. Diffraction-Unlimited All-Optical Imaging and Writing with a Photochromic GFP. *Nature* **2011**, *478*, 204–208.
17. Wiedenmann, J.; Gayda, S.; Adam, V.; Oswald, F.; Nienhaus, K.; Bourgeois, D.; Nienhaus, G. U. From EosFP to mIrisFP: Structure-Based Development of Advanced Photoactivatable Marker Proteins of the GFP-Family. *J. Biophotonics* **2011**, *4*, 377–390.
18. Hoi, H.; Shaner, N. C.; Davidson, M. W.; Cairo, C. W.; Wang, J.; Campbell, R. E. A Monomeric Photoconvertible Fluorescent Protein for Imaging of Dynamic Protein Localization. *J. Mol. Biol.* **2010**, *401*, 776–791.
19. Habuchi, S.; Tsutsui, H.; Kochaniak, A. B.; Miyawaki, A.; van Oijen, A. M. mKikGR, a Monomeric Photoswitchable Fluorescent Protein. *PLoS One* **2008**, *3*, e3944.
20. McEvoy, A. L.; Hoi, H.; Bates, M.; Platonova, E.; Cranfill, P. J.; Baird, M. A.; Davidson, M. W.; Ewers, H.; Liphardt, J.; Campbell, R. E. mMaple: A Photoconvertible Fluorescent Protein for Use in Multiple Imaging Modalities. *PLoS One* **2012**, *7*, e51314.

21. Tsutsui, H.; Karasawa, S.; Shimizu, H.; Nukina, N.; Miyawaki, A. Semi-rational Engineering of a Coral Fluorescent Protein into an Efficient Highlighter. *EMBO Rep.* **2005**, *6*, 233–238.
22. Field, S. F.; Matz, M. V Retracing Evolution of Red Fluorescence in GFP-like Proteins from Faviina Corals. *Mol. Biol. Evol.* **2010**, *27*, 225–233.
23. Adam, V.; Moeyaert, B.; David, C. C.; Mizuno, H.; Lelimousin, M.; Dedecker, P.; Ando, R.; Miyawaki, A.; Michiels, J.; Engelborghs, Y.; *et al.* Rational Design of Photoconvertible and Biphotochromic Fluorescent Proteins for Advanced Microscopy Applications. *Chem. Biol.* **2011**, *18*, 1241–1251.
24. Fuchs, J.; Böhme, S.; Oswald, F.; Hedde, P. N.; Krause, M.; Wiedenmann, J.; Nienhaus, G. U. A Photoactivatable Marker Protein for Pulse-Chase Imaging with Superresolution. *Nat. Methods* **2010**, *7*, 627–630.
25. Adam, V.; Lelimousin, M.; Boehme, S.; Desfonds, G.; Nienhaus, K.; Field, M. J.; Wiedenmann, J.; McSweeney, S.; Nienhaus, G. U.; Bourgeois, D. Structural Characterization of IrisFP, an Optical Highlighter Undergoing Multiple Photo-induced Transformations. *Proc. Natl. Acad. Sci. U.S.A.* **2008**, *105*, 18343–18348.
26. Ando, R.; Mizuno, H.; Miyawaki, A. Regulated Fast Nucleocytoplasmic Shuttling Observed by Reversible Protein Highlighting. *Science* **2004**, *306*, 1370–1373.
27. Kiss, C.; Temirov, J.; Chasteen, L.; Waldo, G. S.; Bradbury, A. R. M. Directed Evolution of an Extremely Stable Fluorescent Protein. *Protein Eng., Des. Sel.* **2009**, *22*, 313–323.
28. Pédelacq, J.-D.; Cabantous, S.; Tran, T.; Terwilliger, T. C.; Waldo, G. S. Engineering and Characterization of a Superfolder Green Fluorescent Protein. *Nat. Biotechnol.* **2006**, *24*, 79–88.
29. Tsutsui, H.; Shimizu, H.; Mizuno, H.; Nukina, N.; Furuta, T.; Miyawaki, A. The E1 Mechanism in Photo-induced Beta-Elimination Reactions for Green-to-Red Conversion of Fluorescent Proteins. *Chem. Biol.* **2009**, *16*, 1140–1147.
30. Lelimousin, M.; Adam, V.; Nienhaus, G. U.; Bourgeois, D.; Field, M. J. Photoconversion of the Fluorescent Protein EosFP: A Hybrid Potential Simulation Study Reveals Intersystem Crossings. *J. Am. Chem. Soc.* **2009**, *131*, 16814–16823.
31. Hayashi, I.; Mizuno, H.; Tong, K. I.; Furuta, T.; Tanaka, F.; Yoshimura, M.; Miyawaki, A.; Ikura, M. Crystallographic Evidence for Water-Assisted Photo-induced Peptide Cleavage in the Stony Coral Fluorescent Protein Kaede. *J. Mol. Biol.* **2007**, *372*, 918–926.
32. Mizuno, H.; Mal, T. K.; Tong, K. I.; Ando, R.; Furuta, T.; Ikura, M.; Miyawaki, A. Photo-induced Peptide Cleavage in the Green-to-Red Conversion of a Fluorescent Protein. *Mol. Cell* **2003**, *12*, 1051–1058.
33. Fron, E.; Van der Auweraer, M.; Moeyaert, B.; Michiels, J.; Mizuno, H.; Hofkens, J.; Adam, V. Revealing the Excited-State Dynamics of the Fluorescent Protein Dendra2. *J. Phys. Chem. B* **2013**, *117*, 2300–2313.
34. Mizuno, H.; Dedecker, P.; Ando, R.; Fukano, T.; Hofkens, J.; Miyawaki, A. Higher Resolution in Localization Microscopy by Slower Switching of a Photochromic Protein. *Photochem. Photobiol. Sci.* **2010**, *9*, 239–248.
35. Nguyen Bich, N.; Moeyaert, B.; Van Hecke, K.; Dedecker, P.; Mizuno, H.; Hofkens, J.; Van Meervelt, L. Structural Basis for the Influence of a Single Mutation K145N on the Oligomerization and Photoswitching Rate of Dronpa. *Acta Crystallogr., Sect. D: Biol. Crystallogr.* **2012**, *68*, 1653–1659.
36. Miyawaki, A.; Ando, R.; Mizuno, H.; Karasawa, S. Fluorescent Protein. U.S. Patent 8,034,614, 2011.
37. Zhang, M.; Chang, H.; Zhang, Y.; Yu, J.; Wu, L.; Ji, W.; Chen, J.; Liu, B.; Lu, J.; Liu, Y.; *et al.* Rational Design of True Monomeric and Bright Photoactivatable Fluorescent Proteins. *Nat. Methods* **2012**, *9*, 727–729.
38. Ando, R.; Hama, H.; Yamamoto-Hino, M.; Mizuno, H.; Miyawaki, A. An Optical Marker Based on the UV-Induced Green-to-Red Photoconversion of a Fluorescent Protein. *Proc. Natl. Acad. Sci. U.S.A.* **2002**, *99*, 12651–12656.
39. Wiedenmann, J.; Ivanchenko, S.; Oswald, F.; Schmitt, F.; Röcker, C.; Salih, A.; Spindler, K.-D.; Nienhaus, G. U. EosFP, a Fluorescent Marker Protein with UV-Inducible Green-to-Red Fluorescence Conversion. *Proc. Natl. Acad. Sci. U.S.A.* **2004**, *101*, 15905–15910.
40. Mizuno, H.; Mal, T. K.; Wälchli, M.; Kikuchi, A.; Fukano, T.; Ando, R.; Jeyakanthan, J.; Taka, J.; Shiro, Y.; Ikura, M.; *et al.* Light-Dependent Regulation of Structural Flexibility in a Photochromic Fluorescent Protein. *Proc. Natl. Acad. Sci. U.S.A.* **2008**, *105*, 9227–9232.
41. Yarbrough, D.; Wachter, R. M.; Kallio, K.; Matz, M. V.; Remington, S. J. Refined Crystal Structure of DsRed, a Red Fluorescent Protein from Coral, at 2.0-Å Resolution. *Proc. Natl. Acad. Sci. U.S.A.* **2001**, *98*, 462–467.
42. Wall, M. A.; Socolich, M.; Ranganathan, R. The Structural Basis for Red Fluorescence in the Tetrameric GFP Homolog DsRed. *Nat. Struct. Biol.* **2000**, *7*, 1133–1138.
43. Quillin, M. L.; Anstrom, D. M.; Shu, X.; O'Leary, S.; Kallio, K.; Chudakov, D. M.; Remington, S. J. Kindling Fluorescent Protein from *Anemonia sulcata*: Dark-State Structure at 1.38 Å Resolution. *Biochemistry* **2005**, *44*, 5774–5787.
44. Andresen, M.; Stiel, A. C.; Trowitzsch, S.; Weber, G.; Eggeling, C.; Wahl, M. C.; Hell, S. W.; Jakobs, S. Structural Basis for Reversible Photoswitching in Dronpa. *Proc. Natl. Acad. Sci. U.S.A.* **2007**, *104*, 13005–13009.
45. Pletnev, S.; Subach, F. V; Dauter, Z.; Wlodawer, A.; Verkhusha, V. V A Structural Basis for Reversible Photoswitching of Absorbance Spectra in Red Fluorescent Protein rsTagRFP. *J. Mol. Biol.* **2012**, *417*, 144–151.
46. Adam, V.; Nienhaus, K.; Bourgeois, D.; Nienhaus, G. U. Structural Basis of Enhanced Photoconversion Yield in Green Fluorescent Protein-like Protein Dendra2. *Biochemistry* **2009**, *48*, 4905–4915.
47. Kim, H.; Grunkemeyer, T. J.; Modi, C.; Chen, L.; Fromme, R.; Matz, M. V.; Wachter, R. M. Acid−Base Catalysis and Crystal Structures of a Least Evolved Ancestral GFP-like Protein Undergoing Green-to-Red Photoconversion. *Biochemistry* **2013**, *52*, 8048–8059.
48. Ando, R.; Flors, C.; Mizuno, H.; Hofkens, J.; Miyawaki, A. Highlighted Generation of Fluorescence Signals Using Simultaneous Two-Color Irradiation on Dronpa Mutants. *Biophys. J.* **2007**, *92*, L97–L99.
49. Dean, K. M.; Lubbeck, J. L.; Binder, J. K.; Schwall, L. R.; Jimenez, R.; Palmer, A. E. Analysis of Red-Fluorescent Proteins Provides Insight into Dark-State Conversion and Photodegradation. *Biophys. J.* **2011**, *101*, 961–969.
50. Gurskaya, N. G.; Verkhusha, V. V; Shcheglov, A. S.; Staroverov, D. B.; Chepurnykh, T. V; Fradkov, A. F.; Lukyanov, S.; Lukyanov, K. A. Engineering of a Monomeric Green-to-Red Photoactivatable Fluorescent Protein Induced by Blue Light. *Nat. Biotechnol.* **2006**, *24*, 461–465.
51. Subach, F. V; Zhang, L.; Gadella, T. W. J.; Gurskaya, N. G.; Lukyanov, K. A.; Verkhusha, V. V. Red Fluorescent Protein with Reversibly Photoswitchable Absorbance for Photochromic FRET. *Chem. Biol.* **2010**, *17*, 745–755.
52. Sawano, A.; Miyawaki, A. Directed Evolution of Green Fluorescent Protein by a New Versatile PCR Strategy for Site-Directed and Semi-random Mutagenesis. *Nucleic Acids Res.* **2000**, *28*, e78.
53. Miyazaki, K.; Takenouchi, M. Creating Random Mutagenesis Libraries Using Megaprimer PCR of Whole Plasmid. *Biotechniques* **2002**, *33*, 1033–10341036−1038.
54. Ward, W. W. Properties of the Coelenterate Green-Fluorescent Proteins. *Bioluminescence and Chemiluminescence: Basic Chemistry and Analytical Applications*; DeLuca, M., McElroy, W. D., Eds.; Academic Press Inc.: New York, 1981; pp 235−242.
55. Iizuka, R.; Yamagishi-Shirasaki, M.; Funatsu, T. Kinetic Study of *De Novo* Chromophore Maturation of Fluorescent Proteins. *Anal. Biochem.* **2011**, *414*, 173–178.
56. Dedecker, P.; Duwé, S.; Neely, R. K.; Zhang, J. Localizer: Fast, Accurate, Open-Source, and Modular Software Package for Superresolution Microscopy. *J. Biomed. Opt.* **2012**, *17*, 126008.